JOURNAL OF MATERIALS SCIENCE 13 (1978) 1217–1223

Crystallization of amorphous (bulk and thin films) $Ge_x Se_{1-x}$ ($0 < x < 0.20$) alloys

M. ESQUERRE, J.C. CARBALLES
LCR Thomson–CSF, Domaine de Corbeville, 91406 Orsay, France

J.P. AUDIERE, C. MAZIERES
Laboratoire de Physicochimie Minérale, Université de Paris Sud, Bâtiment 420, 91405 Orsay, France

Amorphous alloys $Ge_x Se_{1-x}$ ($0 \leqslant x \leqslant 0.20$) have been studied using X-ray diffraction and DTA for bulk material, and X-ray diffraction and optical or scanning electronic microscopy for thin films deposited on quartz. For $x = x_e$ (eutectic composition) ~ 0.10, crystallization during annealing at $T = 190°$ C was never observed in bulk material; it did take place, though slowly, in the films. Annealing of bulk material ($x < 0.10$) leads to phase separation into trigonal Se and a non-crystalline phase, the observed T_g of which increases with the annealing time to a 110° C limit corresponding to the eutectic composition; for $x > 0.10$ annealing produces a separation between $GeSe_2$ (polymorph II) and a non-crystalline phase again of composition x_e, which decomposes afterwards. In the film alloys with $x \lesssim 0.20$, observations under microscope suggests a decomposition of a spinodal type.

1. Introduction

The selenium–germanium system $Ge_x Se_{1-x}$ presents a large range of easy vitrification around the eutectic composition $x_e \sim 0.08$ (Fig. 1). This paper is concerned with the $0 \leqslant x \leqslant 0.20$ range and gives an account of a comparison of the phase separation and the crystallization process in the non-crystalline phases on either side of the $x_e \sim 0.10$ composition for both bulk material and thin film. For bulk materials, the differential thermal analysis (DTA) gives information complementing the previous results [1–3]; for thin films optical or scanning microscopy are invaluable to approach the various aspects of crystallization.

2. Preparation

Selenium (99.99%) and germanium (Johnson Matthey 50 Ω cm) in required proportions were placed in quartz bulbs; the bulbs were vacuum sealed, then heated at 900° C for 24 h in a rocking oven in order to homogenize the material, then dropped in a salt–water–ice mixture; the Ge–Se alloy so quenched was used either as prepared or in a flash evaporation system. The vapour pressure of Ge and Se are very different, and it proved difficult, during the evaporation, to preserve stoichiometry and homogeneity inside the film and on its surface because of thermal radiation. To avoid this drawback a special evaporation crucible was designed (Fig. 2). Made of berylium oxide, this conical crucible ($\phi_{int.max} = 5$ mm) was wound with a tungsten heating wire and enclosed in an alumina box; this arrangement considerably reduced the radiating surfaces and the subsequent re-evaporations of the selenium deposited on the surrounding surfaces. The films obtained in this way, under a pressure $\sim 10^{-6}$ Torr during the evaporation, were about 2% richer in Ge than the starting material; they showed a good bulk and surface homogeneity and reproductibility was also good. Substrates were optically polished quartz discs ($\phi = 30$ mm) and 0.5 mm thick. They were carefully cleaned before use, then attached to a stainless steel substrate bearer whose temperature

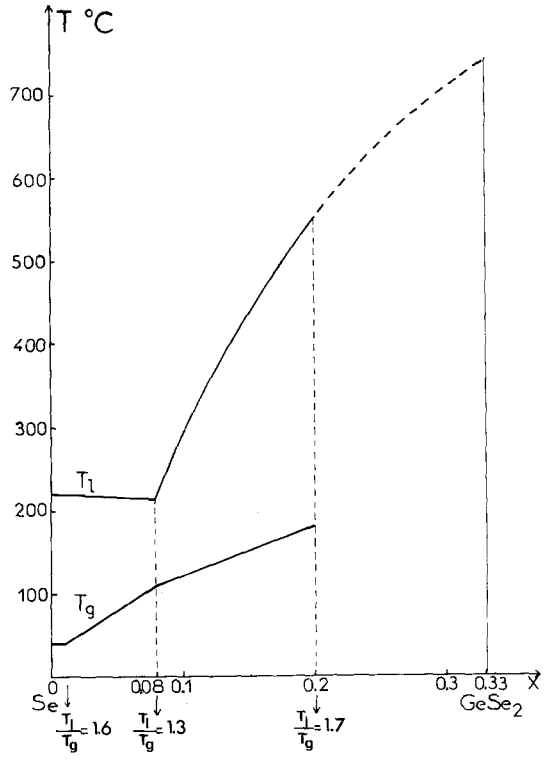

Figure 1 Se–$GeSe_2$ diagram.

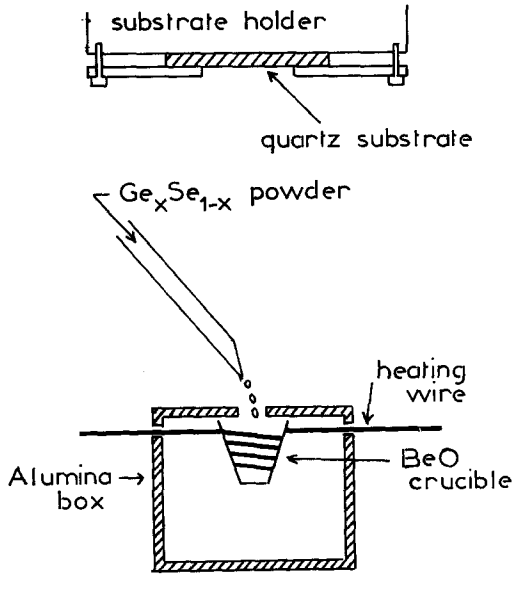

Figure 2 Evaporation system.

could be maintained constant at ±2° C between −180° C and 200° C. During the evaporation, the temperature of the substrate was ~0° C; at this temperature the general aspect of the film was excellent. Film thickness was continuously controlled with piezoelectric quartz scales.

3. Control of the materials

Thermal analysis of the bulk material was performed on a few mg samples placed in specially designed quartz vacuum sealed microbulbs. The stoichiometry of the bulk material and of the thin films was checked by X-fluorescence. The bulk homogeneity was checked with an ion probe (Ar^+ ions) and the Ge/Se ratio was found to be constant at every point inside the sample. After preparation, the thickness e of films with 2000 Å $< e <$ 1 μm was measured by Nomarski optical interferometry (accuracy 10%), while that of films with $e <$ 2000 Å was measured by X-ray interferometry (accuracy 1%). Scanning microscopy was performed after deposition of a gold layer a few angstroms thick on the film to be observed. X-ray diffraction studies were obtained with a Debye–Scherrer camera for bulk material and with a diffractometer for films. The criteria adopted for amorphicity were the following: for all samples, absence of X-diffraction lines; for bulk samples, presence of a DTA crystallization signal; for films, absence of any visible crystallites in microscope observations.

4. Results and interpretation

4.1. Bulk material before annealing

For $0 \leqslant x \leqslant 0.20$, all materials are amorphous. Their thermograms (Fig. 3) show a T_g signal which shifts from ~40° C (pure Se) towards higher temperatures with increasing proportions of Ge, while the signal area decreases. These observed T_g values are in good agreement with [4] and [5]. For $0 \leqslant x \leqslant 0.10$, an endothermic signal appears around 217° C: its area decreases for increasing x and it obviously shows the melting of the selenium crystallized from the amorphous system during the DTA between T_g and 217° C. The crystallization process of this Se is responsible for the "a–b" part of the thermograms and is consistent with the results which follow.

4.2. Annealed bulk material

Annealing of Ge_xSe_{1-x} was achieved in vacuum sealed quartz bulbs. After a 16 day annealing at 190° C (i.e., just below the eutectic temperature) and a 2 h cooling to room temperature, the X-ray routine diagrams showed the results given in Table I.

The modifications of the thermograms after various annealing treatments are quite characteristic (Fig. 4). Annealing the Ge_xSe_{1-x} material

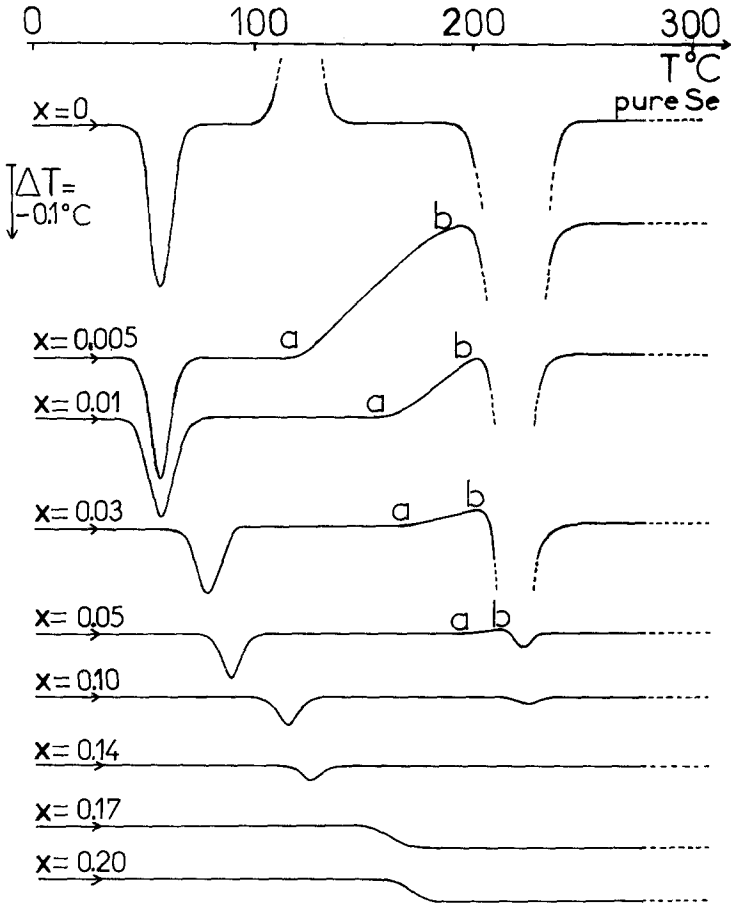

Figure 3 DTA thermograms for bulk Ge_xSe_{1-x} ($0 \leqslant x \leqslant 0.2$), heating rate $16^\circ C\ min^{-1}$.

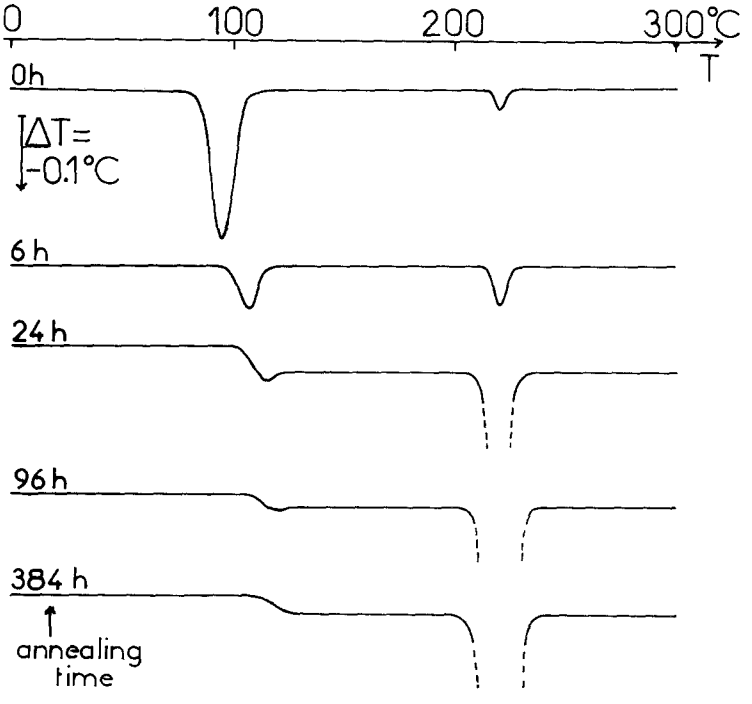

Figure 4 Evolution of DTA thermograms of bulk $Ge_{0.05}Se_{0.95}$ ($x = 0.05$) for different annealing times.

TABLE I

x (Ge at.%)	Observed spectra
0–3	Trigonal Se (sharp lines)
5	Trigonal Se (large rings)
10	No lines or rings
14–20	$GeSe_2$ (polymorph II). Lines consistent with Burgeat [6] and different from Ch'un Hua [7]

with $0 \leqslant x < 0.10$ for increasing times yields a decrease of the T_g signal area, a shift of its temperature towards the limit of 110° C and an increase of the melting signal area at 219° C. The corresponding X-ray diffraction patterns show the progressive appearance of trigonal Se. For $x \sim 0.10$ (eutectic composition) annealing does not modify the thermogram: the constancy of T_g, remaining at 110° C, and the lack of X-ray diffraction lines are clear evidence that the material remains amorphous. Finally, at $0.10 < x < 0.20$, annealing for increasing times decreases the T_g (from 180° C, for example at $x = 0.20$) to the limit of 110° C; meanwhile, the $GeSe_2$(II) diffraction pattern appears.

4.3. Thin films before any annealing

Observations under the microscope either by reflexion or by transmission do not detect any crystallites. No X-ray diffraction lines appear. Therefore all films are considered as non-crystalline.

4.4. Annealed thin films

Films are annealed at 190° C until crystallites are visible under the microscope. The annealing time necessary to reach this threshold depends on x (Fig. 5); the maximum corresponds to $x \sim x_e$.

For $0 < x < 0.05$, red cylindrites appear at the Se–quartz interface (Fig. 6); their diameter increases with increasing annealing time, but not their number. There is obviously heterogenous nucleation at the interface, followed by growth [8]. The red cylindrites are quite characteristic of a typical form of trigonal Se [9], as confirmed by the X-ray patterns.

For compositions close to x_e (in the range 0.07–0.12), dentritic figures grow at the film–quartz interface (Fig. 7) after a minimum annealing time of 400 h. The boundaries of these dendrites remain sharply defined during annealing. Tiny yellow circular crystallites ($\phi \sim 3\,\mu m$) also appear, randomly distributed on the dendrites; the amorphous, orange-coloured matrix is continuously consumed during the annealing. The similarity between the observed crystallization of thin films of pure Se [8] and the X-ray diffraction demonstrate that the dendrites are trigonal Se and that the yellow tiny crystals are $GeSe_2$(II) [6].

On the Ge-rich side of the eutectic composition ($0.14 < x < 0.17$), ~240 hours annealing yields two crystalline phases (Fig. 8) growing inside the amorphous matrix: the yellow one corresponds to $GeSe_2$ (II); the red one is made of dendrites quite

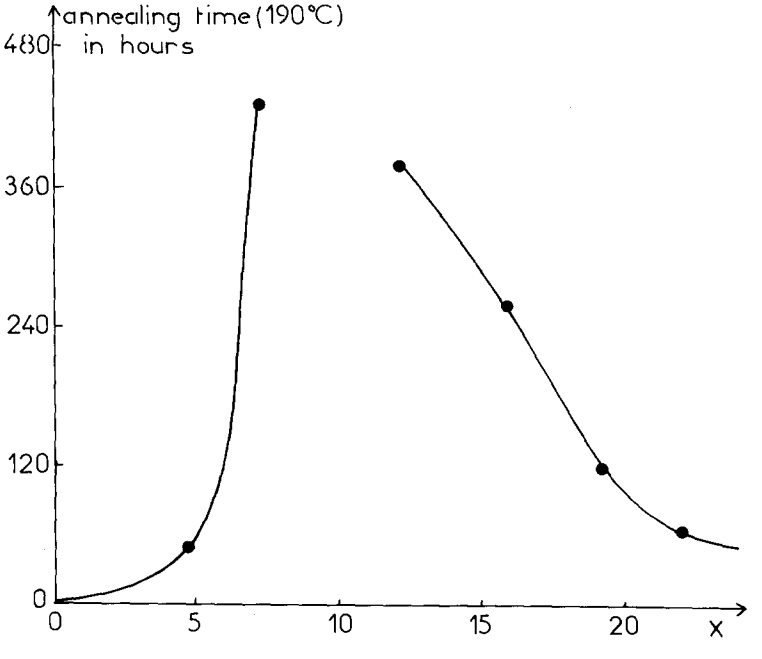

Figure 5 Annealing time (at 190° C) necessary to the observation of crystallites (optic microscopy) in the Ge_xSe_{1-x} thin films.

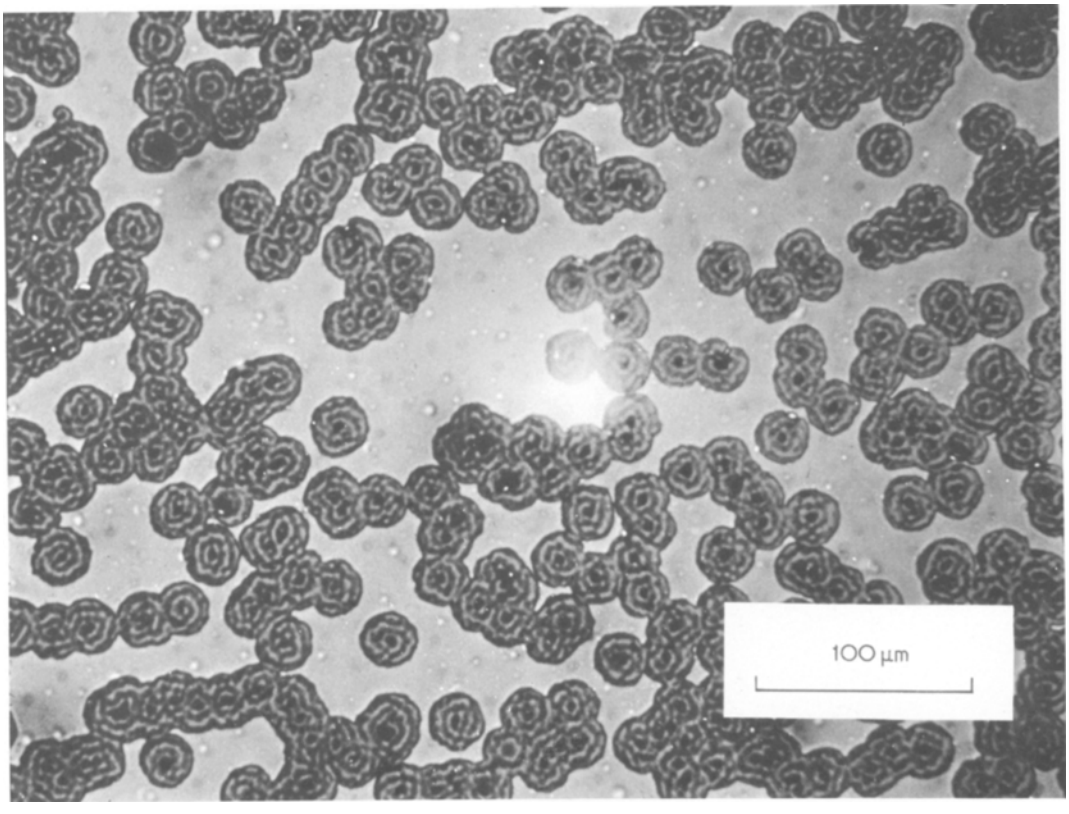

Figure 6 Optical microscopy observation of $Ge_{0.05}Se_{0.95}$ thin film after 72 h annealing (190° C).

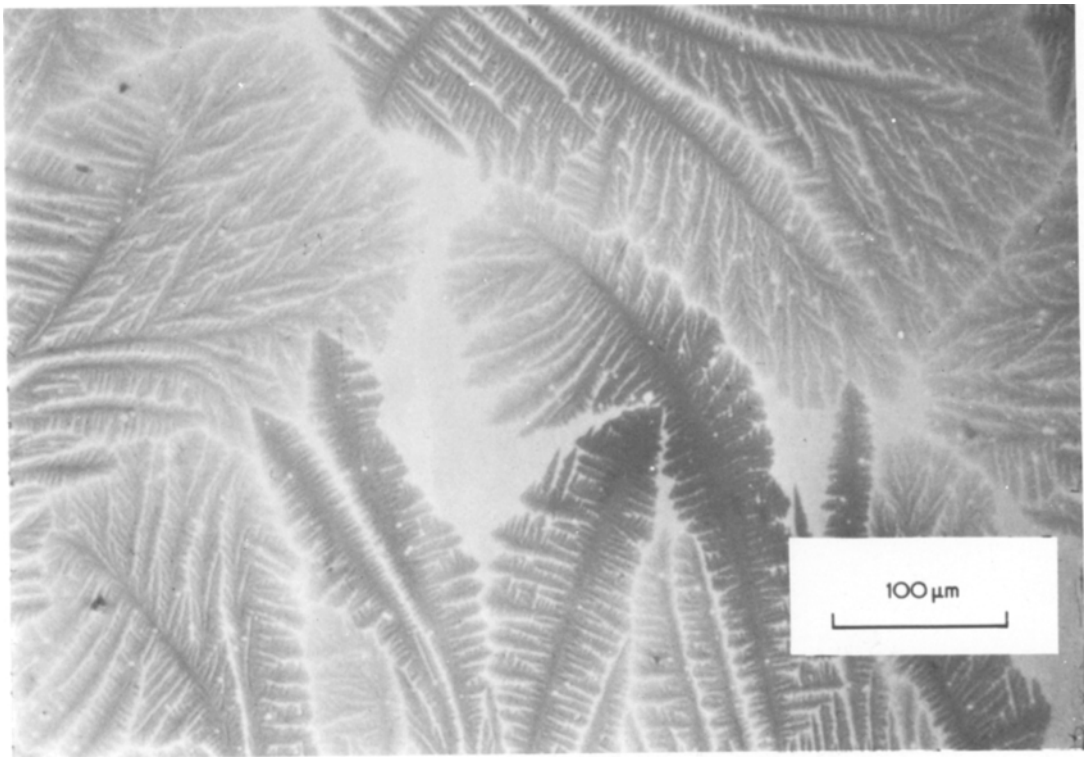

Figure 7 Optical microscopy observation of $Ge_{0.09}Se_{0.91}$ thin film after 430 h annealing (190° C).

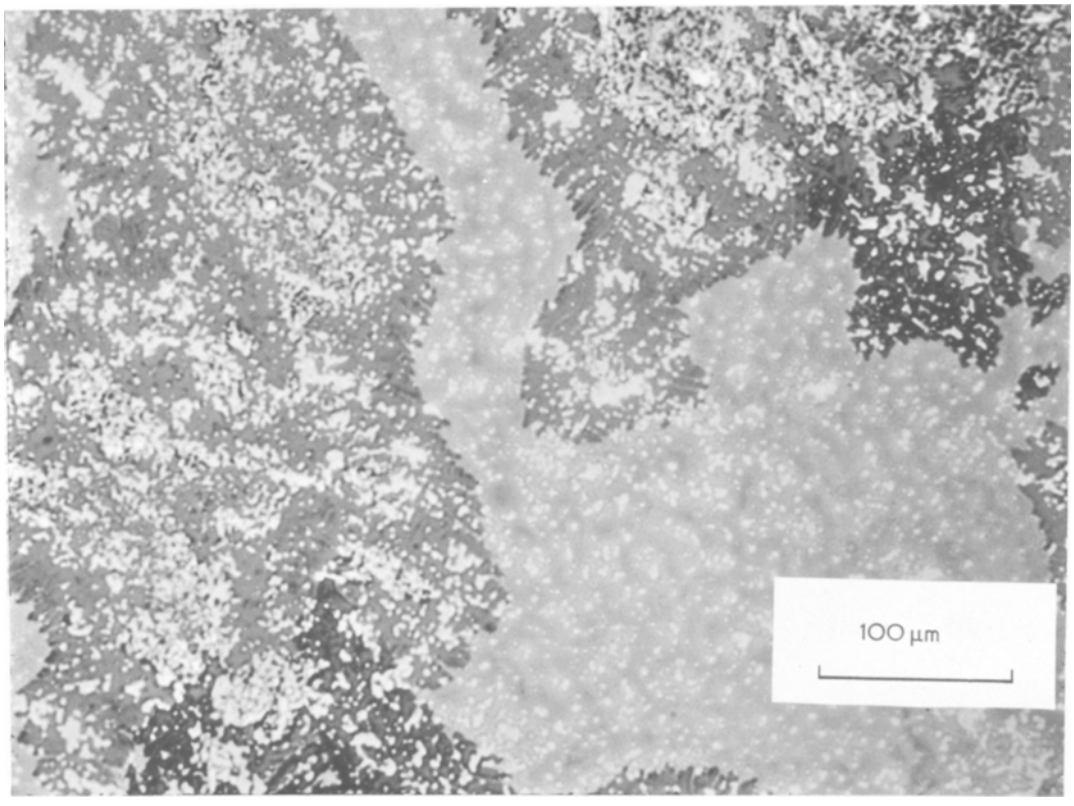

Figure 8 Optical microscopy observation of $Ge_{0.16}Se_{0.84}$ thin film after 240 h annealing (190° C).

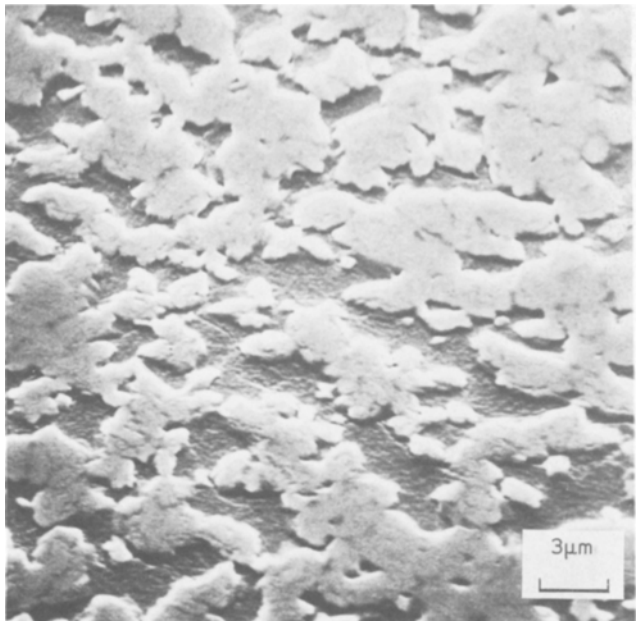

Figure 9 Scanning electronic microscopy observation of $Ge_{0.20}Se_{0.80}$ after 48 h annealing (190° C).

similar to those appearing in the films originally of eutectic composition ($x \sim 0.10$). Increasing the Ge proportion up to $x \sim 0.20$ decreases the time required for the first appearance of crystals under the microscope (Fig. 9) to 48 h. The interfaces are quite diffuse at the beginning of this crystallization, but become more and more clearly defined during annealing. There is a high degree of connectivity between the domains of each phase.

5. Discussion and conclusion

The above results emphasize the very strong glass forming ability (GFA) of the alloys with composition close to x_e, a behaviour consistent with the trend in many binary systems. However, some less common features are observed in the present one: for x increasing from 0 to x_e and to $x = 0.2$, the T_g of unannealed materials is also continuously increasing from 40° C to 110° C and 180° C respectively (Fig. 1). This is not surprising [12] in the range $0.08 < x < 0.2$ where the liquidus temperature increases from 218° C to 550° C, but it raises questions in the range $0 < x < x_e$ where T_l is roughly constant. Annealing the thin films samples in this range of composition yields cylindrites of Se starting at the interface defects, while the matrix remains non-crystalline and increasingly rich in Ge up to a concentration close to x_e as suggested by the evolution of T_g (Fig. 4). It would appear that some Se_n species are mobile enough to separate themselves from the amorphous alloy, provided that the concentration of Ge in the alloy is smaller than x_e; trigonal Se then crystallizes.

The T_g of the amorphous phase does not change appreciably (~40° C as for pure Se) as long as Ge < 0.01, however when $x \gtrsim 0.01$ it starts to increase and reachs 110° C for $x \sim x_e$. The ratio T_l/T_g thus changes from 1.6 ($x = 0.01$) to 1.3 ($x = 0.08$) and this decrease is accompanied by an increasing GFA. Such behaviour is consistent, but of course does not explain why, T_l remaining almost constant, the viscosity of the non-crystalline alloy at a given temperature below T_l increases when x increases from 0.01 to 0.08. One can think that an increasing number of Ge atoms cause a more effective blockage of the motions of Se_n species. On the other hand, the cohesion energy of the crystalline phases Se + $GeSe_2$ (II) (in thermodynamic equilibrium below T_l, at these concentrations) is not affected, since T_l is almost constant. Fig. 10 offers a tentative scheme for the evolution of the free enthalpy of the non-crystalline phase, as prepared, in the investigated system. It is drawn making the assumption that the tendency to crystallize parallels the evolution of the difference ΔG between the crystalline and the non-crystalline systems; an assumption which is of course, very crude since it neglects the kinetic barriers in the crystallization process. The very strong GFA at $x \sim x_e$ decreases more rapidly on the $x < x_e$ side than on the $x > x_e$ side (Fig. 4). On this side, the G_{am} curve should present a spinode around $x \sim 0.14$ if photographs such as (Fig. 9) are taken as an indication of an eventual spinodal decomposition.

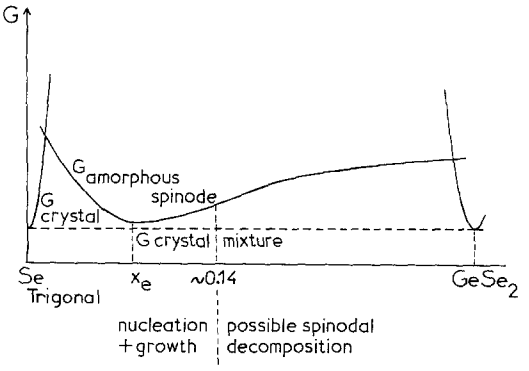

Figure 10 Tentative free energy G versus composition schematic diagram.

References

1. A. BRENAC, Journées d'information sur l'élaboration des composés semiconducteurs amorphes et cristallins, CNET edit. **A** (1974) No. 1341.
2. P. TRONC, M. BENSOUSSAN and A. BRENAC, *Phys. Rev.* **B 8-12** (1973) 5947.
3. R. AZOULAY, H. THIBERGE and A. BRENAC, *J. Non-Cryst. Solids* **18.1** (1975) 33.
4. A. DEMBROVSKII, C. Z. VINOGRADOVA and A. S. PASHINKIN, *Rus. J. Inorg. Chem.* **10** (1965) 903.
5. J. P. AUDIERE, J. C. CARBALLES and C. MAZIERES, *J. Therm. Anal.* **6** (1974) 27.
6. J. BURGEAT, G. LE ROUX and A. BRENAC, *J. Appl. Cryst.* **8** (1975) 325.
7. C. H. LIU, A. S. PASHINKIN and A. V. NOVOSELOVA, *Dokl. Akad. Nauk SSSR*, **146** (1962) 1092.
8. R. CLEMENT, J. C. CARBALLES and B. de CREMOUX, J. *Non-Cryst. Solids* **15** (1974) 505.
9. J. P. AUDIERE, C. MAZIERES and J. C. CARBALLES, *ibid.* **27** (1978) 411.
10. J. W. CAHN, *Trans. Met. Soc. Aime* **242** (1968) 166.
11. K. S. KIM and D. TURNBULL *J. Appl. Phys.* **44** (1973) 5237.
12. *Idem, ibid.* **45** (1974) 3447.
13. S. SAKKA and J. D. MACKENZIE, *J. Non-Cryst. Solids* **6** (1971) 145.

Received 9 August 1977 and accepted 21 September 1977.